Reactive Inflight Obstacle Avoidance via Radar Feedback*

Kartik B. Ariyur†, Peter Lommel and Dale F. Enns

Abstract— **Avoidance of unmapped obstacles is critical to autonomous flight in forested areas and urban canyons. The small vehicles capable of navigating in these spaces necessarily cannot carry the heavy and sophisticated sensor packages carried on large aircraft. We propose simple reactive feedback laws that enable obstacle avoidance for a hover-capable unmanned aerial vehicle (UAV) using a crude low resolution, small field of view radar sensor. The basic component in these laws is the reduction in the velocity component in the direction of the obstacle. We illustrate the performance of these feedback laws on a point mass double integrator model with velocity and acceleration limits. Simulation results in both 2-D and 3-D settings are presented.**

I. INTRODUCTION

The use of Unmanned Aerial Vehicles (UAVs) for surveillance dates back to the US Army's SD-1/RP-71 in the 1950s and the modified Firebee used in the Vietnam war [4]. In recent times, more ambitious goals are envisaged for these vehicles– close-up surveillance of urban, forested or mountainous terrain in battle, and law enforcement. To permit reconnaisance of complex terrains without a concomitant increase in personnel needed, autonomous flight is essential. There are however several roadblocks: first, complete topographic information of these Areas of Operation (AOs) is unavailable or unobtainable in advance (e.g., a clothesline/new phone line/power line or antenna in a street); second, the available information may not be accurate; third, the global positioning system (GPS) absolute position sensors on these vehicles can lose accuracy or completely lose the GPS signal in complex terrain. There is thus a need for reactive maneuvering using feedback from relative position sensors. Relative position can be determined using vision, acoustic or electromagnetic ranging sensors. Acoustic sensors are range limited; vision systems provide highly accurate sensing but are highly sensitive to atmospheric conditions–dust, smoke, fog, clouds and precipitation; simple radars provide long range and robustness to atmospheric conditions but provide limited resolution and field of view (FOV).

Similar problems have been addressed before in other circumstances. There is a rich literature in robotics on iterative learning control, where robots extract and use the topography of their operating environs through repeated traversal [3]. There is also a variety of path planning algorithms for uncertain environments [5], [6], [7]. Work on automated highways has resulted in obstacle avoidance methods in quasi 1-D problems [2]. Here, automobiles use fast sensing of recognizable patterns (e.g., the tail-lights of the car in front). Nevertheless, autonomous flight throws up challenges unmet by existing methods: limited actuation authority is distributed in three dimensions as opposed to practically one for ground robots and automobiles; fast execution of tasks is not only desirable but necessary (especially in battlefields); operation is seldom repeated in the same region for many of the anticipated applications; the flying vehicle is much more of a safety risk to operators.

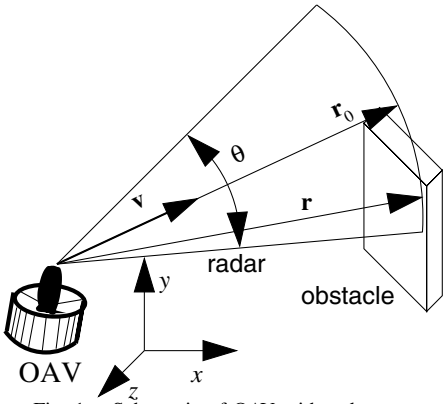

Fig. 1. Schematic of OAV with radar sensor

This work was motivated by the DARPA Organic Air Vehicle (OAV) program where we built a 29 inch diameter ducted fan vehicle (similar to the vehicle analyzed in [1]). The avoidance of gimbals for sensors (to reduce mechanical complexity/increase reliability) and the payload limits of the OAV platform resulted in our considering the use of feedback from a crude light radar for obstacle avoidance. We propose simple feedback laws to *correct directly the local velocity command to the vehicle*, rather than replanning the path. These laws owe their origin to the problem of avoiding a single obstacle in the field of view. We illustrate their performance for flight in multi-obstacle fields–they perform well so long as there aren't too many obstacles in the FOV.

Section II presents the point mass model and its nominal tracking control laws, Section III presents the basic velocity command modification and its variants in two dimensions, Section IV presents three dimensional variants of the schemes in Section III, Section V describes simulation results in a variety of situations and Section VI provides concluding remarks.

II. POINT MASS MODEL AND NOMINAL CONTROL

We develop obstacle avoidance for a double integrator point mass model using a radar of range $r_{max} = 15$m (50ft)

*This work was supported by Honeywell AES

†Corresponding author. Kartik B. Ariyur and Dale F. Enns are with the Honeywell Labs, 3660 Technology Dr., Minneapolis, MN 55418. Email: kartik.ariyur@honeywell.com, dale.f.enns@honeywell.com

Peter Lommel was with Honeywell Labs when he performed this work, and is currently with the Draper Lab at MIT. phlommel@mit.edu

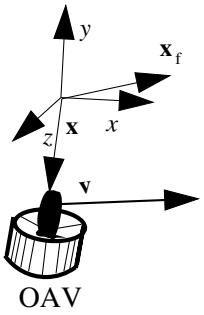

Fig. 2. Nominal tracking

and a $\theta = 40^\circ$ FOV angle with a (low) angular resolution of 40° (see the schematic in Figure 1). The radar cone is assumed to point in the direction of the vehicle velocity. An obstacle detected with such a radar at some position $\mathbf{r}$ relative to the vehicle is detected as being along the velocity vector $\mathbf{v}$, i.e., along $\mathbf{r}_0$ in Figure 1–it will be different if the radar resolution were finer than the its FOV. The point mass model has the advantage of simplicity and captures the essential properties of an aircraft with attitude stabilization. Indeed, use of feedback linearization or dynamic inversion for attitude stabilization makes the tracking dynamics appear as a series of integrators. For the OAV, the use of dynamic inversion in the inner loop results in the tracking dynamics appearing as a point mass model with saturations.

We formally posit the model below for both 2D and 3D:

$$\ddot{\mathbf{x}} = \mathbf{a}_{cmd}, \tag{1}$$

where $\mathbf{x} = [x \quad y]^T$, $\mathbf{a}_{cmd} = [a_x \quad a_y]^T$ in 2D, and $\mathbf{x} = [x \quad y \quad z]^T$, $\mathbf{a}_{cmd} = [a_x \quad a_y \quad a_z]^T$ in 3D. The limits on acceleration and velocity are as follows:

$$\begin{aligned} \|\mathbf{v}\| &\leq v_{max}, \quad \mathbf{v} = \dot{\mathbf{x}} && (2)\\ \|\mathbf{a}_{cmd}\| &\leq a_{max}. && (3) \end{aligned}$$

Typically, the velocity limits and acceleration limits for an aerial vehicle are different for the different cartesian components, and the saturation surface is not spherical as we have posited here for simplicity. However, our feedback laws can be easily extended to these cases.

We next posit the nominal tracking control laws for the point mass model; these ensure exponentially stable tracking to the destination $\mathbf{x}_f$ in Figure 2 when there are no obstacles. The acceleration and velocity commands are given as follows:

$$\mathbf{a}_{cmd} = \begin{cases} \frac{\mathbf{v}_{cmd}-\mathbf{v}}{\tau_\mathbf{v}} & \|\frac{\mathbf{v}_{cmd}-\mathbf{v}}{\tau_\mathbf{v}}\| \leq a_{max} \\ a_{max}\frac{\frac{\mathbf{v}_{cmd}-\mathbf{v}}{\tau_\mathbf{v}}}{\|\frac{\mathbf{v}_{cmd}-\mathbf{v}}{\tau_\mathbf{v}}\|} & \|\frac{\mathbf{v}_{cmd}-\mathbf{v}}{\tau_\mathbf{v}}\| > a_{max} \end{cases} \tag{4}$$

$$\mathbf{v}_{cmd}^{nom} = \frac{\mathbf{x}_f - \mathbf{x}}{\tau_\mathbf{x}}, \tag{5}$$

where $\tau_\mathbf{v}$ and $\tau_\mathbf{x}$ are the velocity and position time constants respectively, $\mathbf{v}_{cmd}^{nom}$ is the nominal velocity command, $\mathbf{v}_{cmd}$ is the actual velocity command derived from the nominal command and obstacle avoidance considerations.

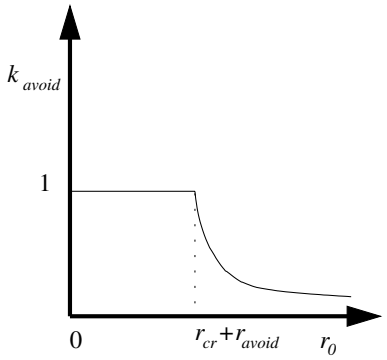

Fig. 3. Collision avoidance gain

III. VELOCITY COMMAND MODIFICATION

The basic velocity command modification is performed if an obstacle is within the range and field of view of the radar, and there is a positive component of vehicle velocity command along the current velocity vector (which, from the previous section is taken as the direction toward the obstacle as the resolution of the radar and its field of view are the same). This basic modification to the nominal velocity command is the same in both 2D and 3D; it consists in subtracting the component of the nominal velocity command in the direction of the obstacle–

$$\begin{aligned} \mathbf{v}_{cmd}^{mod} &= \mathbf{v}_{cmd}^{nom} - k_{avoid}\,(\mathbf{v}_{cmd}^{nom}\cdot\mathbf{r}_0)\,\mathbf{e}_0 && (6)\\ k_{avoid} &= \min\left\{1, e^{-\|\mathbf{r}_0\|+r_{cr}+r_{avoid}}\right\} && (7)\\ \mathbf{e}_0 &= \frac{\mathbf{r}_0}{\|\mathbf{r}_0\|}, \quad r_{cr} = \frac{(\mathbf{v}\cdot\mathbf{e}_0)^2}{2a_{max}}, && (8) \end{aligned}$$

where r_{avoid} is a preferred minimum distance from the obstacle determined for example, from the navigation envelope of the vehicle. The critical distance r_{cr} is the closest that the vehicle can come to an obstacle and still decelerate to a stop without collision. In the case where the FOV angle and resolution of the radar are identical, $r_{cr} = \frac{\|\mathbf{v}\|^2}{2a_{max}}$. The critical distance r_{cr} can also be calculated using the nominal commanded velocity as $r_{cr} = \frac{(\mathbf{v}_{cmd}^{nom}\cdot\mathbf{e}_0)^2}{2a_{max}}$ to provide a more conservative estimate. Finally, the overall commanded velocity $\mathbf{v}_{cmd}$ has the form

$$\mathbf{v}_{cmd} = \mathbf{v}_{cmd} + \mathbf{v}_c, \tag{9}$$

where $\mathbf{v}_c$ is used to ensure that $\mathbf{v}_{cmd}$ does not remain zero and also for imposing desired characteristics upon the trajectory.

We now proceed to explain the construction of the gain k_{avoid} in Eqn. (6). First, we note that $k_{avoid} \in [0,1]$ always: it is less than unity when the obstacle is farther than $r_{cr} + r_{avoid}$, and unity when closer. Figure 3 plots k_{avoid} as a function of distance from an obstacle.

We consider three forms for the command augmentation $\mathbf{v}_c$ in the 2D case:

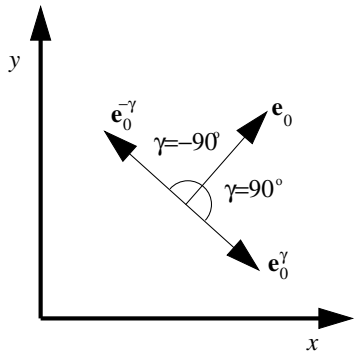

Fig. 4. Turn command addition

1) **Random command addition.** This is performed when $\|\mathbf{v}\| < v_{min}$, i.e., the velocity falls below a small value. This addition is of the form

$$\mathbf{v}_c = v_{mag} \begin{bmatrix} n_1 \\ n_2 \end{bmatrix}, \tag{10}$$

where $v_{mag} < v_{max}$, and $\begin{bmatrix} n_1 \\ n_2 \end{bmatrix}$ is a unit vector of random orientation in the plane. This method is suited for the avoidance of point obstacles, i.e., obstacles whose relevant dimensions are smaller than the view dimension of the radar $r_{max}\theta$. Trees and pillars, and other large aspect ratio obstacles fall in this category.

2) **Systematic turn command addition.** The random command addition presented above can result in long residence time near a large obstacle such as a large wall. This method eliminates this possibility through consistently turning left or right to follow the boundary of the obstacle. It is of the form:

$$\mathbf{v}_c = v_{mag}\mathbf{e}_0^{\gamma} \tag{11}$$

$$\mathbf{e}_0^{\gamma} = \begin{bmatrix} \cos\gamma & \sin\gamma \\ -\sin\gamma & \cos\gamma \end{bmatrix} \mathbf{e}_0, \tag{12}$$

where $\gamma > \theta$ the FOV angle of the radar, and $v_{mag} < v_{max}$. Positive or negative γ results in clockwise or counter-clockwise rotation respectively. When $\gamma = \mp 90^\circ$, we have the case of full right or left turns as illustrated in Figure 4.

3) **A safe method.** This involves decelerating to a stop once an obstacle is in sight and within critical range, and then move in a perpendicular direction $\gamma = 90^\circ$ with full control authority.

IV. VELOCITY COMMAND MODIFICATION IN 3D

While the basic command modification in 3D is the same as in Eqn. (6), there is greater freedom in choice of the command augmentation. While we can use a command addition in the direction of a randomly oriented unit vector similar to the random command addition presented in Section III, the other command augmentations are not as straightforward. A systematic augmentation $\mathbf{v}_c = v_{mag}\mathbf{e}_0^{\gamma}$ at an angle γ under the constraint $\mathbf{e}_0^{\gamma} \cdot \mathbf{e}_0 = \cos\gamma$ results in any of a multiplicity of directions on a right circular cone with semi-angle γ and axis along $\mathbf{r}_0$. To get over this redundancy, we can optimize one of the components of $\mathbf{e}_0^{\gamma}$ or a function of the components. For example, maximization of the z-component of $\mathbf{e}_0^{\gamma}$ results in

$$\mathbf{e}_0^{\gamma} = \begin{bmatrix} \frac{\mp e_{0x}e_{0y}\sin\gamma + e_{0x}cos\gamma\sqrt{1-e_{0z}^2}}{\sqrt{1-e_{0z}^2}} \\ \frac{\mp e_{0y}e_{0z}\sin\gamma + e_{0y}cos\gamma\sqrt{1-e_{0z}^2}}{\sqrt{1-e_{0z}^2}} \\ \pm\sqrt{1-e_{0z}^2}\sin\gamma + e_{0z}cos\gamma \end{bmatrix}, \tag{13}$$

where $\mathbf{e}_0 = [e_{0x}\ e_{0y}\ e_{0z}]^T$, and $e_{0z} \neq 1$. If $e_{0z} = 1$, then there is no further maximization possible. We investigated a few other strategies for 3D obstacle avoidance. The first is to obtain a direction in a plane perpendicular to the velocity (which is in the direction of the obstacle detected). The velocity command augmentation in this case is given as follows:

$$\mathbf{v}_c = v_{mag}\mathbf{e}_0^{\gamma,\perp} \tag{14}$$

$$\mathbf{e}_0^{\gamma,\perp} = \frac{\mathbf{e}_0^{\gamma} \times \mathbf{e}_0}{\|\mathbf{e}_0^{\gamma} \times \mathbf{e}_0\|}, \tag{15}$$

where the magnitude $v_{mag} < v_{\max}$. This method is of value when there is a variety of truly 3D features in the obstacle field. Another reactive command augmentation is to simply decelerate to hover, climb to a height where the obstacle is no longer in the sensor's field of view and then continue to the destination. This is motivated by situations where most of the obstacles (such as buildings in a small town or village) are of small height. Finally, simple deceleration and systematic turn command addition can be combined to produce a control law that guarantees safety–use the turn command addition when farther than critical distance $r_{cr} + r_{avoid}$ and use the decelerate to stop-hover-climb strategy when closer.

V. SIMULATION RESULTS

This section supplies some simulation studies of the simple reactive obstacle avoidance control laws in complex obstacle fields. The following model parameters were used in the simulations for the nominal closed loop waypoint tracking: maximum acceleration and velocity limits of $a_{\max} = 3\text{ms}^{-2}$ and $v_{\max} = 3\text{ms}^{-1}$; velocity and position time constants $\tau_{\mathbf{v}} = 0.5\text{s}$ and $\tau_{\mathbf{x}} = 0.25\text{s}$; and an avoid distance $r_{avoid} = 1\text{m}$. The radar sensor was implemented in 2D as a circular sector with angle $\theta = 40^\circ$ and radius 15m, and in 3D as a spherical sector with the cone angle θ. In the case of both point obstacles and polygonal/prism obstacles, only the range to the nearest obstacle is used by the feedback laws. In all of the simulations, the basic velocity command modification posited in Eqn. (6) is performed. The simulations were performed in MATLAB and SIMULINK.

Figure 5 shows a traversal through an obstacle field of random points (to simulate a forest of trees) from $(0,35)$

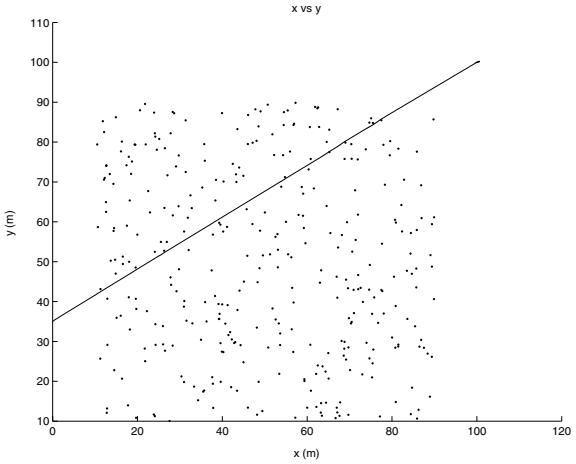

Fig. 5. Random command addition

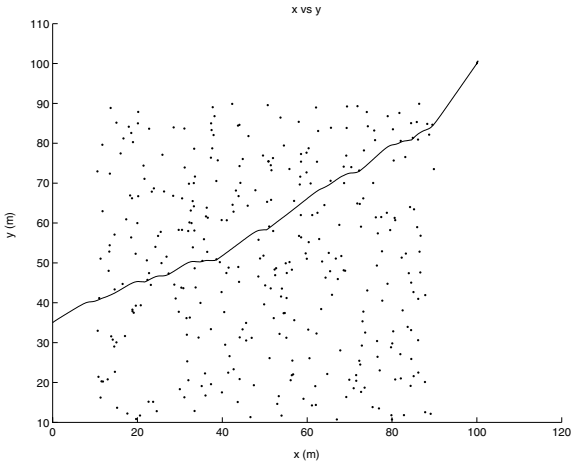

Fig. 6. Systematic turn addition, $\gamma = 90^\circ$

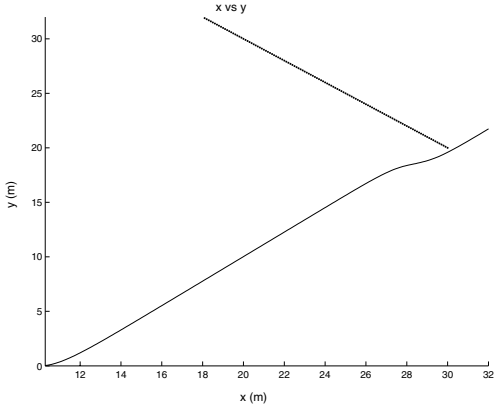

Fig. 7. Systematic turn addition, $\gamma = 90^\circ$: large obstacle

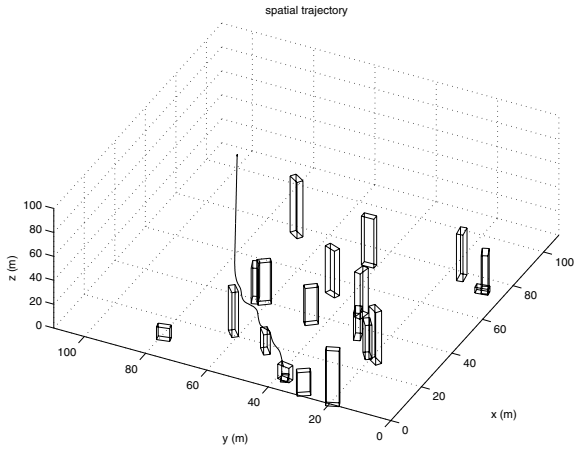

Fig. 8. 3D obstacle avoidance: systematic ccw turn

to $(100,100)$ using the random command addition given in Eqn. (10). The trajectory appears straight on the scale of this figure–the minimum miss distance to obstacles on the trajectory was as small as 0.4m, less than the preferrred avoid distance of $r_{avoid} = 1$m. This is because the vehicle has a narrow FOV and limited range, and the obstacle avoidance was designed for single obstacles; not for multiple obstacles in the FOV. Random velocity command augmentation is used only when the velocity goes below 0.1ms^{-1}.

Figure 6 shows use of the systematic turn right strategy using the velocity command augmentation in Eqn. (11) with $\gamma = 90^\circ$. The initial and final posiitions are the same as in Figure 5. The path is longer in this case than in the previous case where random command addition is used. This is because the obstacles are distributed randomly and the vehicle keeps turning right to avoid them.

Figure 7 shows the avoidance of a continuous obstacle such as a wall using the same turn right strategy. The initial position in this case is at $(10,0)$. For long obstacles such as walls which can completely obscure the FOV of the sensor, a random command addition can potentially keep the vehicle oscillating near the wall. The strategy of keeping right or left avoids this possibility.

We now describe in detail a simulation of 3D obstacle avoidance. Figure 8 shows the path of the vehicle (starting from $(0,35,20)$) under the velocity augmentation given by Eqn. 14. Here, $\mathbf{e}_0^{\gamma}$ is calculated using Eqn. (13) to maximize the z-component, with $\gamma = 40^\circ$, and $\mathbf{e}_0^{\gamma,\perp}$ is calculated using Eqn. (15). Figure 9 plots the position histories of its coordinates. The method is successful in obstacle avoidance in this sparse obstacle field, and others we tested it on. It begins to break down when the obstacles become dense–pointing to a need for better sensor resolution or a larger FOV angle. Figure 10 shows the histories of velocity components and Figure 11 the histories of acceleration components.

VI. CONCLUSIONS

We have developed simple reactive control laws that are computable in milliseconds and provide obstacle avoidance in a variety of situations using just a crude low resolution radar sensor. The simple structure of these feedback control laws make them amenable to analysis. While the methods need the vehicle to decelerate to a stop or to a small velocity repeatedly, and slow down the traversal, a hovering vehicle can easily perform these maneuvers. We are investigating

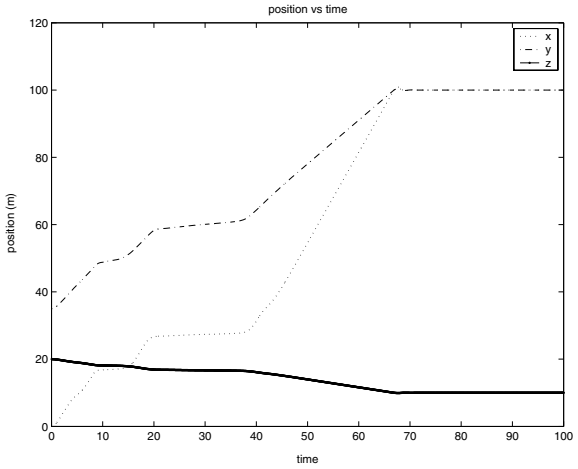

Fig. 9. 3D obstacle avoidance: position history

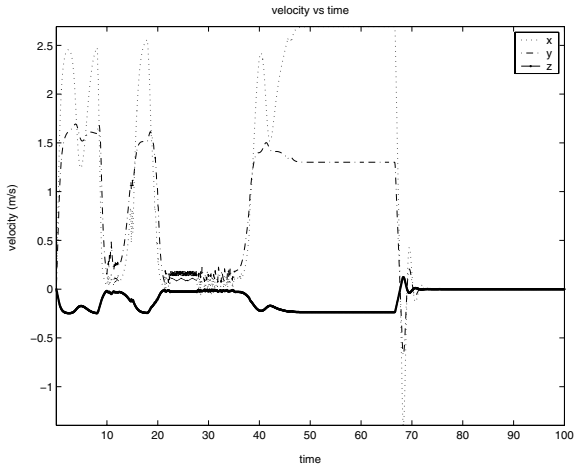

Fig. 10. 3D obstacle avoidance: velocity history

the conditions under which these methods or their variants can supply obstacle avoidance guarantees under suitable conditions on the range sensor and the vehicle navigation envelope.

VII. ACKNOWLEDGMENTS

We thank Datta Godbole, Mike Jackson and Steve Pratt for useful discussions.

REFERENCES

[1] J. Fleming, T. Jones, J. Lusardi, P. Gelhausen, D. Enns, "Improved control of ducted fan VTOL UAVs in crosswind turbulence," *AHS International 4th Decennial Specialists' Conference on Aeromechanics*,pp. 17–28, 2004.

[2] D. N. Godbole, V. Hagenmeyer, R. Sengupta, D. Swaroop, "Design of emergency maneuvers for automated highway system: obstacle avoidance problem," *Proceedings of the 36th IEEE Conference on Decision and Control*, pp. 4774–4779, San Diego, CA, USA, 1997.

[3] K. Moore and J.-X. Xu Guest Eds., Special Issue on Iterative Learning Control, *International Journal of Control*, Vol.73, No.10, 2000.

[4] L. R. Newcome, *Unmanned Aviation: A Brief History of Unmanned Aerial Vehicles*, AIAA, Reston, VA, 2004.

[5] A. Stentz,"The focussed $D*$ algorithm for real-time replanning," *Proceedings of the International Joint Conference on Artificial Intelligence*, August 1995.

[6] A. Stentz,"Optimal and efficient path planning for partially-known environments," *Proceedings of the IEEE International Conference on Robotics and Automation*, May 1994.

[7] L. L. Whitcomb and D. E. Koditschek,"Automatic assembly planning and control via potential functions," Proceedings of the IEEE/RSJ International Workshop on Intelligent Robots and Systems, 1991.

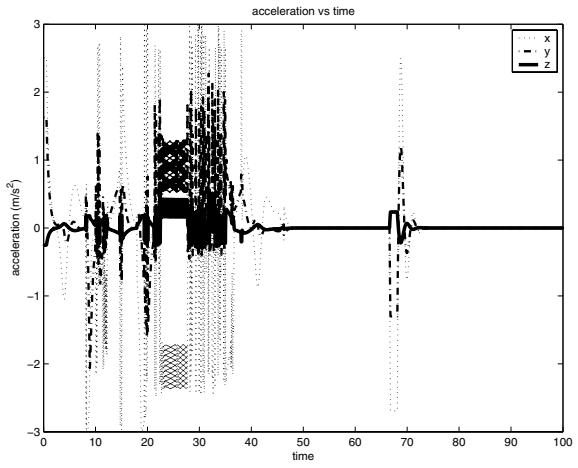

Fig. 11. 3D obstacle avoidance: acceleration history